From Yellow to Black: Dramatic changes between Ce(IV) and Pu(IV) Molybdates

Justin N. Cross, Patrick M. Duncan, Eric M. Villa, Matthew J. Polinski, Jean-Marie Babo, Evgeny V. Alekseev, Corwin H. Booth, Thomas E. Albrecht-Schmitt[*]

Department of Chemistry and Biochemistry, Florida State University, 95 Chieftan Way, 310 DLC, Tallahassee, Florida 32306-4390

Department of Chemistry and Biochemistry and Department of Civil Engineering and Geological Sciences, University of Notre Dame, 156 Fitzpatrick Hall, University of Notre Dame, Notre Dame, Indiana 46556; Fax: (+01)574-631-9236

Institute for Energy and Climate Research (IEK-6), Forschungszentrum Jülich GmbH, 52428 Jülich, Germany;

Institut für Kristallographie, RWTH Aachen University, 52066 Aachen, Germany

Chemical Sciences Division, Lawrence Berkeley National Laboratory, Berkeley, CA 94720

E-mail: talbrechtschmitt@gmail.com

RECEIVED DATE (to be automatically inserted after your manuscript is accepted if required according to the journal that you are submitting your paper to)

Abstract: Hydrothermal reactions of $CeCl_3$ and $PuCl_3$ with MoO_3 and Cs_2CO_3 yield surprisingly different results. $Ce_3Mo_6O_{24}(H_2O)_4$ crystallizes as bright yellow plates, space group *C*2/*c* *a* = 12.7337(7) Å, *b* = 22.1309(16) Å, *c* = 7.8392(4) Å, β = 96.591(4)º, V = 2194.6(2) Å^3; whereas $CsPu_3Mo_6O_{24}(H_2O)$ crystallizes as semi-conducting black-red plates, space group *C*2/*c*, *a* = 12.633(5) Å, *b* = 21.770(8) Å, *c* = 7.743(7) Å, β = 96.218(2)º, V = 2117(2) Å^3. The topologies of the two compounds are similar with channel structures built from disordered Mo(VI) square pyramids and REO_8 square anti-prisms (RE = Ce(IV) or Pu(IV)). However, the Pu(IV) compound contains Cs^+ in its channels, while the channels in $Ce_3Mo_6O_{24}(H_2O)_4$ contain water molecules. Disorder and an ambiguous oxidation state of Mo lead to the formula $CsPu_3Mo_6O_{24}(H_2O)$ where one Mo site is Mo(V) and the rest are Mo(VI). X-ray absorption near-edge structure (XANES) experiments were performed to investigate the source of the black color of $CsPu_3Mo_6O_{24}(H_2O)$. These experiments revealed Pu to be tetravalent while the strong pre-edge absorption from the distorted molybdate anions leaves the oxidation state ambiguous between Mo(V) and Mo(VI).

Keywords: actinide molybdate • cerium • plutonium • optical energy spectrum • semiconductor • XANES

Introduction

The term surrogate has been widely applied to the use of non- or less-radioactive elements in the place of shorter-lived isotopes that are more challenging to investigate. This replacement is particularly common with plutonium where Ce(IV) has been used to replace Pu(IV), and Nd(III) has been used to replace Pu(III). This substitution is based on nearly identical ionic radii and the chemistry is in fact often very similar. In an effort to move away from the use of surrogates in actinide chemistry, recent studies have clearly shown the differences between lanthanide and actinide compounds when they are synthesized under similar conditions. In the trivalent state, the rare earth borate series has displayed significant structural differences between the lanthanides and actinides both in the local coordination of

the metal center and the borate network.[1-3] Computational studies of these systems reveals that the differences in structures and local coordination environments are a direct consequence of covalency between the 6*p* or 6*d* orbitals and ligand orbitals with Pu(III), Am(III), and Cm(III); a feature that is completely absent in lanthanides. In the tetravalent state, discrepancies have been shown between Ce(IV) and Pu(IV) as well as between early An(IV) and transuranic An(IV).[4-14] Exploration of this field is filled with opportunity as there are only a few systems that have systematically spanned the lanthanide and actinide series such as the aquo-triflates, phosphonates, and phosphites.[15-25] It is in this objective we have chosen to explore the rare earth molybdates.

Molybdenum oxoanions are well known to be highly distorted due to second-order Jahn-Teller effects that give rise to a Mo(VI) center that can adopt several different geometries. Molybdates can be octahedral, square pyramidal, trigonal bipyramidal, and tetrahedral. The adoption of coordination geometries lacking an inversion center makes it an attractive ligand to produce noncentrosymmetric compounds.[26-33] In addition, Mo^{VI}–O bonds are highly polarizable like borate, and therefore differences in reactivity between Pu(IV) and Ce(IV) may be realized if this polarization of electron density leads to covalent bonding even if the effects are minor. Furthermore, much like borate, molybdate can form polymeric networks that are likely to rearrange as a consequence of metal complexation. What differentiates molybdate from borate is that it is redox active and stabilizes Pu(IV) instead of Pu(III).

Molybdates are also important to the spent nuclear fuel cycle. Molybdenum is a fission product and the formation of plutonium molybdates has been suggested as a means of creating insoluble products from the dissolution of breached zirconium clad fuel rod limiting the mobility Pu into the environment.[34] Molybdate phases also form from the alteration of spent nuclear fuel during burn-up and have a large impact on the mobility of all actinides in a repository-type environment.[35]

The environmental importance and structural complexity of molybdate has driven a large research effort in the structural chemistry of actinyl molybdates and to a smaller extent the trivalent and tetravalent actinide molybdates.[36-41] Concurrently, lanthanide molybdates have also been investigated for their complex and interesting properties such as negative thermal expansion, ferroelectricity,

ferroelasticity, photoluminescence, and interesting structure types.[42-49] Of particular interest is the compound Ce_2MoO_6 of the Ln_2MoO_6 series (Ln = La – Lu). Ce_2MoO_6 is unusual with respect to the rest of the series as it adopts a black color while the others assume their typical colors and appears to adopt a structure unique to the series. Its anomalous properties were attributed to mixed valency either from Ce or Mo.[50-51] Soderholm et al. carried out a series of investigations on Ce_2MoO_6 to determine the valance state of both Ce and Mo using X-ray absorbance measurements and to determine accurate unit cell constants using neutron diffraction. They found that within the limits of their experiment all Ce was trivalent and all the molybdenum was hexavalent attributing the properties to oxygen vacancies.[52-54] Herein we report a new Pu(IV) molybdate of black color, $CsPu_3Mo_6O_{24}(H_2O$, which contrasts greatly with its congener Ce(IV) in the bright yellow $Ce_3Mo_6O_{24}(H_2O)_4$. Although both share similar reaction paths, oxidizing from RE(III) to RE(IV), and structural topologies consisting of channel structures built of disordered molybdate square pyramids, the similarities end there. We use RE in this work to describe Ce and Pu for ease of understanding and simplicity. The actinides are traditionally not considered rare earths, but contemporarily they have been described as such. The channels of $Ce_3Mo_6O_{24}(H_2O)_4$ contain water molecules whereas the channels of $CsPu_3Mo_6O_{24}(H_2O)$ contain Cs^+ cations. Additionally, the plutonium compound is a semi-conductor with a band-gap of 1.20 ± 0.03 eV while the cerium compound is wide band-gap semi-conductor with a gap of 2.68 ± 0.02 eV.

Experimental Section

Syntheses. $CeCl_3$ (99.9%, Alfa Aesar), Cs_2CO_3 (99.9%, Alfa Aesar) were all used as obtained. Weapons grade plutonium (94% ^{239}Pu, 6% ^{240}Pu) in the form of $PuCl_3$ was used as received from LANL. Reactions were run in PTFE-lined Parr 4749 autoclaves with a 23 mL internal volume for the lanthanides, and with a 10 mL internal volume autoclave for plutonium. Deionized water was used in all reactions. *Caution! ^{239}Pu ($t_{1/2}$ = 24,065 y) and ^{240}Pu ($t_{1/2}$ = 6,537 y) represent serious health risks owing to their α and γ emission. All studies with plutonium were conducted in a laboratory dedicated to studies on transuranium elements. This laboratory is located in a nuclear science facility and is equipped with*

a HEPA filtered hoods and negative pressure gloveboxes that are ported directly into the hoods. A series of counters continually monitor radiation levels in the laboratory. The laboratory is licensed by the Nuclear Regulatory Commission. All experiments were carried out with approved safety operating procedures. All free-flowing solids are worked with in gloveboxes, and products are only examined when coated with either water or Krytox oil and water. There are significant limitations in accurately determining yield with plutonium compounds because this requires drying, isolating, and weighing a solid, which poses certain risks, as well as manipulation difficulties given the small quantities employed in the reactions.

$CsPu_3Mo_6O_{24}(H_2O)$. $PuCl_3$ (0.0105 g, 0.0301 mmol), MoO_3 (0.005 g 0.0343 mmol), Cs_2CO_3 (0.0071 g, 0.022 mmol), and 150 µL of H_2O were loaded into a 10 mL autoclave. The autoclave was sealed and heated to 200 °C in a box furnace in an argon-filled glovebox for five days. The autoclave was then cooled down to room temperature at a rate of 5 °C/h. The products were rinsed with water and thin black plates were isolated.

$Ce_3Mo_6O_{24}(H_2O)_4$. $CeCl_3$ (0.0493 g, 0.200 mmol), MoO_3 (0.0287g 0.200 mmol), Cs_2CO_3 (0.652 g, 0.200 mmol), and 2.0 mL of H_2O were loaded into a 23 mL autoclave. The autoclave was sealed and heated to 200 °C in a box furnace for five days. The autoclave was then cooled down to room temperature at a rate of 5 °C/h. The products were rinsed with water and yellow acicular crystals were isolated. Yellow plates were also obtained from this reaction, however suitable crystals for SCXRD could not be found. Similar results were obtained substituting K_2CO_3 for Cs_2CO_3. It was found that addition of one molar equivalent of a mild oxidizing agent such as $Te(OH)_6$ increased the yield.

Crystallographic Studies. Single crystals of $CsPu_3Mo_6O_{24}(H_2O)$ and $Ce_3Mo_6O_{24}(H_2O)_4$ were mounted on cryoloops with viscous Krytox and optically aligned on a Bruker APEXII Quazar X-ray diffractometer using a digital camera. Initial intensity measurements were performed using a IµS X-ray source (MoKα, λ =0.71073 Å) with high-brilliance and high-performance focusing Quazar multilayer optics. Standard APEXII software was used for determination of the unit cells and data collection control. The intensities of reflections of a sphere were collected by a combination of multiple sets of

exposures (frames). Each set had a different φ angle for the crystal and each exposure covered a range of 0.5° in ω. For $Ce_3Mo_6O_{24}(H_2O)_4$ a total of 2762 images with an exposure time of 20 seconds were collected. For $CsPu_3Mo_6O_{24}(H_2O)$ a total of 1464 images with an exposure time of 40 seconds were collected. The SAINT software was used for data integration including Lorentz and polarization corrections. Both crystals were non-merohedrally twinned with a rotation angle of 180°. The program CELL_NOW was used to de-twin the data. Multi-Scan absorption corrections were applied using the program TWINABS.[55]

UV-vis-NIR Spectroscopy. UV-vis-NIR data were acquired from single or twinned crystals using a Craic Technologies microspectrophotometer. Crystals were placed on quartz slides under Krytox oil, and the data was collected from 200 to 1200 nm for $CsPu_3Mo_6O_{24}(H_2O)$ and 200 to 950 nm for $Ce_3Mo_6O_{24}(H_2O)_4$.

SEM-EDS Analysis. Scanning electron microscopy/energy-dispersive spectroscopy (SEM/EDS) images and data were collected using a LEO Model EVO 50 system with an Oxford INCA energy-dispersive spectrometer. EDS indicated a 1:3:6 ratio of Cs:Pu:Mo for the crystals of $CsPu_3Mo_6O_{24}(H_2O)$ and a 1:2 ratio of Ce:Mo for $Ce_3Mo_6O_{24}(H_2O)_4$.

X-ray Absorption Studies. A crystalline sample of $CsPu_3Mo_6O_{24}(H_2O)$ was mounted in a triply-nested slotted aluminum frame with sealed kapton windows for the X-ray absorption studies. Spectra were measured at the Stanford Synchrotron Radiation Lightsource on beamline 11-2 using a half-tuned double Si(220) (ϕ=0°) monochromator with 0.3 mm wide vertical slits. Data were collected in fluorescence mode using a 30-element Ge detector, and all spectra were corrected for dead-time effects.

Results and Discussion

Structure and Topological Description.

$CsPu_3Mo_6O_{24}(H_2O)$ and $Ce_3Mo_6O_{24}(H_2O)_4$ both crystallize in the space group *C*2/*c* and share similar topologies. The main feature of both structures is the channels that extend along the *c*-axis. In

$Ce_3Mo_6O_{24}(H_2O)_4$ these channels house water molecules; whereas in $CsPu_3Mo_6O_{24}(H_2O)$ the channels are smaller by approximately 1 Å across and contain disordered Cs^+ cations as shown in Figure 1. The difference in channel size is reflected in the smaller volume of $CsPu_3Mo_6O_{24}(H_2O)$ at 2117(2) $Å^3$ versus $Ce_3Mo_6O_{24}(H_2O)$ at 2194.6(2) $Å^3$ The two structures each contain two unique RE atoms which are coordinated by eight O atoms forming square antiprisms with approximate D_{4d} symmetry.[12,56] All O atoms in the REO_8 polyhedra are donated from molybdate units. The REO_8 polyhedra edge share to form chains continuing down the *c* axis. The edge sharing alternates between aligning with the [*ac*] and [*bc*] planes between each polyhedra as shown for both $CsPu_3Mo_6O_{24}(H_2O)$ and $Ce_3Mo_6O_{24}(H_2O)_4$ in Figure 2. The average bond distances for the $Pu(1)O_8$ and $Pu(2)O_8$ polyhedra are 2.326(9) Å and 2.341(9) Å, respectively. The average bond distances for the $Ce(1)O_8$ and $Ce(2)O_8$ polyhedra are both 2.338(6) Å. The molybdate oxoanions for both structures consist of MoO_5 square pyramids with the Mo(2) and Mo(3) sites disordered over two positions through a 180° rotation. These disordered sites are approximately 75%/25% occupied for Mo(2A)/Mo(2B) and approximately 85%/15% for Mo(3A)/Mo(3B) sites in both studied structures. The Mo–O distances in $Mo(1)O_5$ groups are presented by two short (1.66(1) - 1.77(1) Å), one intermediate (1.86(7) Å), and two normal (1.94(1) – 2.09(1) Å) bonds. $Mo(2A)O_5$ is quite similar with $Mo(1)O_5$ and consists of two short (1.61(1) – 1.79(1) Å), one intermediate (1.882(9) Å) and two normal (2.01(1) – 2.09(1) Å) Mo – O bonds. $Mo(3A)O_5$ groups are based on two short (1.68(1) – 1.78(1) Å), one intermediate (1.831(6) – 1.884(9) Å), one normal (1.93(1) -1.94(1) Å), and one long (2.112(9) – 2.134(6) Å) Mo – O distances. The Mo(B) sites have been left out of the analysis for clarity. In $Ce_3Mo_6O_{24}(H_2O)_4$ Mo(1) edge shares with Mo(3) to form a dimer and Mo(2) edge shares with itself to also form a dimer. It would appear that Mo(3A) corner shares with Mo(2B) through O(13) but O(13) is disordered over two sites as well. This could indicate that they are not oriented towards each other at the same time. Bond valence sums (BVS) are calculations using measured bond distances and predetermined bond valence parameters to determine the valence state of atoms in solid-state chemistry. BVS for Ce indicates a tetravalent oxidation state and BVS for all Mo sites indicate a hexavalent oxidation state (S1).[57] In $CsPu_3Mo_6O_{24}(H_2O)$ there are a similar topologies

for Mo(1), Mo(2A), and Mo(3A) to $Ce_3Mo_6O_{24}(H_2O)_4$, however the Mo(B) sites are different. To begin, the Mo – Mo disordered distances are larger by approximately 0.4 Å for Mo(2) and 0.09 Å for Mo(3). Additionally, Mo(3B), instead of Mo(3A), appears to corner share with Mo(2B) this interaction is again through the disordered O(13) but the O(13) disorder distance is twice as long as it was in $Ce_3Mo_6O_{24}(H_2O)_4$ leading O(13B) to be disordered over a symmetry position. A comparison of molybdate coordination is shown in Figure 3. The BVS calculation for Pu in $CsPu_3Mo_6O_{24}(H_2O)$ indicates tetravalent Pu while Mo BVS indicates hexavalent for all Mo sites except Mo(3B), which indicates Mo(V), however, the disordered O atoms make confident BVS assignments difficult. We have chosen to write the formula as it is shown with one Mo being pentavalent while the rest are hexavalent while making the disordered O13 a water molecule since it has surplus electron density. BVS could not be used to locate any H atoms on O(13) because of the disorder. Writing the formula this way also highlights the placement of Cs in the channels instead of water as it is needed to charge balance the pentavalent Mo. Addition of H atoms to compensate for disordered molybdate anions has been previously reported.[58-60]

UV-Vis-NIR absorption spectroscopy. The absorption spectra for $CsPu_3Mo_6O_{24}(H_2O)$ was obtained from a very thin twinned crystal and is shown in Figure 4. The optical energy spectra for $CsPu_3Mo_6O_{24}(H_2O)$ was obtained from a larger twinned crystal and is shown in Figure 5. The electronic transitions of f-elements are well known and have been characterized in literature, however, the usual analysis fails here because of the dark color and very strong absorbance across the visible spectrum. However, the characteristic bands for Pu(IV) centered around 650 nm and 700 nm can be seen. Typical spectra of Pu(III) and Pu(IV) are found in the supporting information (S2). Using the absorbance data absorbance vs. optical energy plots were constructed to analyze the semi-conductor nature of $CsPu_3Mo_6O_{24}(H_2O)$ as shown in Figure 5. The absorption energy curve was used to estimate the band gap at approximately 1.20 ± 0.03 eV by constructing a linear plot along the steep drop in absorbance highlighted in pink in Figure 5. The x-intercept was then calculated from the equation of the constructed

line. The absorption data of $Ce_3Mo_6O_{24}(H_2O)_4$ was similarly converted to optical energy and the absorbance data can be found in the supporting information (S3 and S4). The bandgap of $CsPu_3Mo_6O_{24}(H_2O)$ is smaller than the 1.8 eV bandgap of PuO_2 but larger than the 0.55 eV bandgap of Pu_2O_2X (X = S, Se).[61-62] The band-gap for $Ce_3Mo_6O_{24}(H_2O)_4$ is much larger than $CsPu_3Mo_6O_{24}(H_2O)$ at 2.68 ± 0.02 eV.

XANES. Pu L3-edge XANES data for both the $CsPu_3Mo_6O_{24}(H_2O)$ crystal and the PuO_2 standard are shown in Fig. 6. The spectra are energy calibrated by setting the energy of the first inflection point of the PuO_2 standard to 18062.3 eV.[63] The strong similarity between the data from the $CsPu_3Mo_6O_{24}(H_2O)$ crystal and PuO_2 indicates that the Pu in the $CsPu_3Mo_6O_{24}(H_2O)$ crystal is predominantly tetravalent Pu(IV). Note that the difference in the peak height of the main "white line" feature between the samples is commonly assigned to differences in the long-range electronic structure due to periodicity, and is not indicative of a difference in valence.

The Mo K-edge XANES are shown in Fig. 7 for the same crystal and a Mo foil standard. The energy is calibrated by setting the first inflection point from the Mo foil data to 20000.36 eV.[64] A large pre-edge feature labeled "A" is observed at 20006.6 eV, and the 1/2-height is at about 20015.eV. There is also a feature "B" at 20027(1) eV and the white line is at about 20042(1) eV (broad and flat compared to "A").

The literature shows that while the Mo K edge is a typically good diagnostic for valence determination when the local geometry is relatively ordered, the large octahedral distortions that can occur around Mo can create very substantial pre-edge features (as observed here) that are far enough up on the main edge that the edge position as given by the position at the first inflection point is no longer very reliable for determining valence differences between Mo(V) and Mo(VI).[65-73] However, the energy at the 1/2-height of the edge is better, and indicates something close to Mo(VI), since Mo(IV) ½-height energies are typically below 20011 eV when using our chosen energy calibration.[63,64] With such uncertainty, it is not really possible to determine how much Mo(V) is mixed in; we therefore report here that the Mo K-edge XANES are consistent with a Mo(V,VI) state.

Conclusions

Two new rare earth molybdates $Ce_3Mo_6O_{24}(H_2O)_4$ and $CsPu_3Mo_6O_{24}(H_2O)$ have been prepared hydrothermally and characterized. Although the two compounds have similar structural topologies there are significant differences between the two compounds. $CsPu_3Mo_6O_{24}(H_2O)$ crystallizes as dark black-red plates that are semiconducting in nature; whereas $Ce_3Mo_6O_{24}(H_2O)_4$ crystallizes as bright yellow tablets with the typical wide gaps of insulating rare earth oxoanion compounds. Large channels are found in both compounds that house H_2O molecules in $Ce_3Mo_6O_{24}(H_2O)_4$ or Cs^+ cations in $CsPu_3Mo_6O_{24}(H_2O)$. X-ray absorption studies were undertaken to determine if mixed oxidation states were the reason for the black color of $CsPu_3Mo_6O_{24}(H_2O)$. XANES clearly indicates a tetravalent state for Pu; however, the distortion away from an octahedral geometry in Mo leads to large pre-edge absorption that prevented a definitive interrogation of the effective nuclear charge of the Mo ions. However, mixed-valent molybdenum is the most likely explanation for the dark color and explains the necessity of filling the channels with Cs^+ cations for charge compensation. This work represents a rather dramatic case where Ce(IV) does not properly model the behavior of Pu(IV). This particular example is quite different from others because previous deviations are observed in the local coordination environments of the rare earth cations which include changes in coordination number, types of ligands, and site symmetry. Rather here, a different redox pathway yields mixed-valency in the anionic network while the local environments of the Ce(IV) and Pu(IV) are virtually indistinguishable.

Acknowledgments

We are grateful for support provided by the Materials Science of Actinides, an Energy Frontier Research Center funded by the U.S. Department of Energy (DOE), Office of Science (OS), Office of Basic Energy Sciences (OBES) under Award Number DE-SC0001089. Work at Lawrence Berkeley National Laboratory supported by the Director, OS, OBES of DOE under Contract No. DE-AC02-

05CH11231. X-ray absorption data were collected at the Stanford Synchrotron Radiation Lightsource, a national user facility operated by Stanford University on behalf of the DOE, OBES. Work the Institute for Climate Research (IEK-6) and Energy Funded by Helmholtz Association Grant VH-NG-815.

Supporting Information

Crystallographic information and calculated BVS values. This material is available free of charge at http://pubs.acs.org.

References

1. Polinski, M. J.; Wang, S.; Alekseev, E. V.; Depmeier, W.; Albrecht-Schmitt, T. E. *Angew. Chem. Int. Ed.* **2011**, 50, 8891-8894.
2. Polinski, M. J.; Grant, D.J.; Wang, S.; Alekseev, E. V.; Cross, J.N.; Villa, E.M.; Depmeier, W.; Gagliardi, L.; Albrecht-Schmitt, T. E. *J. Am. Chem. Soc.* **2012**, 134, 10682-10692.
3. Polinski, M. J.; Wang, S.; Cross, J.N.; Alekseev, E. V.; Depmeier, W.; Albrecht-Schmitt, T. E. *Inorg. Chem.* **2012**, 51, 7859 – 7866.
4. Nelson, A.-G. D.; Bray, T. H.; Zhan, W.; Haire, R.G.; Sayler, T.S.; Albrecht-Schmitt, T.E. *Inorg. Chem.* **2008**, 47, 4945 – 4951.
5. Diwu, J.; Nelson, A.-G. D.; Albrecht-Schmitt, T.E. *Comments. Inorg. Chem.* **2010**, 31, (112), 46-62.
6. Diwu, J.; Nelson, A.-G. D.; Wang, S.; Albrecht-Schmitt, T.E. *Inorg. Chem.* **2010**, 49, 3337-3342.
7. Diwu, J.; Wang, S.; Liao, Z.; Burns, P.C.; Albrecht-Schmitt, T.E. *Inorg. Chem.* **2010**, 49, 10074-10080.
8. Diwu, J.; Wang, S.; Good, J.; Di Stefano, V.H.; Albrecht-Schmitt, T.E. *Inorg. Chem.* **2011**, 50, 4842-4850.
9. Diwu, J.; Good, J.; Di Stefano, V.H.; Albrecht-Schmitt, T.E. *Eur. J. Inorg. Chem.* **2011**, 9, 1374-1377.
10. Diwu, J.; Wang, S.; Albrecht-Schmitt, T.E. *Inorg. Chem.* **2012**, 51, 4088-4093.

11. Gorden, A. E. V.; Shuh, D. K.; Tiedemann, B. E. F.; Wilson, R. E.; Xu, J.; Raymond, K. N. *Chemistry.* **2005**, 11, 2842-2848.

12. Gorden, A. E. V.; Xu, J.; Raymond, K. N. *Chem. Rev.* **2003**, 103, 4207-4282.

13. Xu, J.; Radkov, E.; Ziegler, M.; Raymond, K. N. *Inorg. Chem.* **2000**, 39, 4156-4164.

14. Szigethy, G.; Xu, J.; Gorden, A. E. V.; Teat, S. J.; Shuh, D. K.; Raymond, K. N. *Eur. J. Inorg. Chem.* **2008**, 13, 2143-2147.

15. Burns, J. H.; Peterson, J. R. *Acta Crystallogr.* **1970**, B26, 1885−1887.

16. Burns, J. H.; Peterson, J. R.; Stevenson, J. N. *J. Inorg. Nucl. Chem.* **1975**, 37, 743−749.

17. Matonic, J. H.; Scott, B. L.; Neu, M. P. *Inorg. Chem.* **2001**, 40, 2638−2639.

18. Lindqvist-Reis, P.; Apostolidis, C.; Rebizant, J.; Morgenstern, A.; Klenze, R.; Walter, O.; Fanghaenel, T.; Haire, R. G. *Angew. Chem., Int. Ed.* **2007**, 46, 919−922.

19. Apostolidis, C.; Schimmelpfennig, B.; Magnani, N.; Lindqvist-Reis, P.; Walter, O.; Sykora, R.; Morgenstern, A.; Colineau, E.; Caciuffo, R.; Klenze, R.; Haire, R. G.; Rebizant, J.; Bruchertseifer, F.; Fanghanel, T. *Angew. Chem., Int. Ed.* **2010**, 49, 343−6347.

20. Peterson, J. R.; Burns, J. H. *J. Inorg. Nucl. Chem.* **1973**, 35, 1525−1530.

21. Milman, V.; Winkler, B.; Pickard, C. J. *J. Nucl. Mater.* **2003**, 322, 165−179.

22. Sykora, R. E.; Assefa, Z.; Haire, R. G.; Albrecht-Schmitt, T. E. *J. Solid State Chem.* **2004**, 177, 4413−4419.

23. Assefa, Z.; Haire, R. G.; Sykora, R. E. *J. Solid State Chem.* **2008**, 181, 382−391.

24. Skanthakumar, S.; Antonio, M. R.; Wilson, R. E.; Soderholm, L. *Inorg. Chem.* **2007**, 46, 3485−3491.

25. Cross, J.N.; Villa, E.M.; Wang, S.; Diwu, J.; Polinski, M.J.; Albrecht-Schmitt, T.E. *Inorg. Chem.* **2012**, 51, 8419-8424.

26. Opik, U.; Pryce, M. H. L. *Proc. R. Soc. London* **1937**, A161, 220.

27. Wheeler, R. A.; Whangbo, M. H.; Hughbanks, T.; Hoffman, R.; Burdett, J. K.; Albright, T. A. *J. Am. Chem. Soc.* **1986**, 108, 2222-2236.

28. Pearson, R. G. *J. Mol. Struct.* **1983**, 103, 25-30.

29. Kang, S. K.; Tang, H.; Albright, T. A. *J. Am. Chem. Soc.* **1993**, 115, 1971-1981.

30. Cohen, R. E. *Nature* **1992**, 358, 136-138.

31. Burdett, J. K. *Molecular Shapes*; Wiley-Interscience: New York, **1980**.

32. Kunz, M.; Brown, I. D. J. *Solid State Chem.* **1995**, 115, 395-406.

33. Halasyamani, P. S.; Poeppelmeier, K. R. *Chem. Mater.* **1998**, 10, 2753-2769.

34. Penneman, R.A.; Haire, R.G.; Lloyd, M.H. *ACS Symposium Series*, **1980**, 117, edited by Navratil, J.D. and Schulz, W.W. pp. 57 -58. Washington, DC: American Chemical Society.

35. Buck, E.C.; Wronkiewicz, D.J.; Finn, P.A.; Bates, J.K. *J. Nucl. Mater.* **1997**, 249, 70.-76

36. Krivovichev, S.V.; Burns, P.C. *Structural Chemistry of Inorganic Actinides*; Elsevier: Amsterdam, **2007**, ch. 4, 95.

37. Pages, M.; Freundlich, W. *J. Inorg. Nucl. Chem.* **1972**, 34, 2797-2801.

38. Tabuteau, A.; Pages, M.; Freundlich, W. *Mater. Res. Bull.* **1972**, 7, 691-697.

39. Tabuteau, A.; Pages, M. *J. Solid State Chem.* **1978**, 26, 153-158.

40. Tabuteau, A.; Thevenin, T.; Pages, M. *Rev. Chim. Miner.* **1982**, 19, 173-176.

41. Dahale, N.D.; Keskar, M.; Mudher, S.K.D. *J. Alloys Compd.* **2006**, 415, 244-250.

42. Evans, J. S. O. *J. Chem. Soc., Dalton Trans.* **1999**, 3317-3326.

43. Jeitschko, W *Acta Crystallogr., Sect. B* **1972**, 28, 60-76.

44. Abrahams, S. C.; Svensson, C.; Bernstein, J. L. *J. Chem. Phys.* **1980**, 72, 4278-4286.

45. Hartenbach, I.; Strobel, S.; Dorhout, P.K.; Schleid, T. *J. Solid State Chem.* **2008**, 181, 2828-2836.

46. Hartenbach, I.; Strobel, S.; Dorhout, P.K.; Nockermann, P.; Binnemans, K.; Schleid, T. *Inorg. Chem.* **2008**, 47, 3728-3735.

47. Hartenbach, I.; Strobel, S.; Schleid, T.; Kramer, K.W.; Dorhout, P.K.; *Z. Anorg. Allg. Chem.* **2009**, 635, 966-975.

48. Schleid, T.; Hartenbach, I. *Z. Anorg. Allg. Chem.* **2009**, 635, 1904-1909.

49. Hartenbach, I.; Strobel, S.; Schleid, T.; Dorhout, P.K.; *Z. Anorg. Allg. Chem.* **2010**, 636, 1183-1189.

50. Brixner, L.H.; Sleight, A.W.; Licis, M.S. *J. Solid State Chem.* **1972**, 5, 186-190.

51. Manthiram, A.; Gopalakrishnan, J. *J. Less-Common Met.* **1984**, 99, 107-111.

52. Antonio, M.R.; Xue, J. S.; Soderholm, L. *J. Alloys. Compd.* **1994**, 207/208, 444-448.

53. Antonio, M.R.; Staub, U.; Xue, J. S.; Soderholm, L. *Chem. Mater.* **1996**, 8, 2673-2680.

54. Antonio, M.R.; Xue, J. S.; Soderholm, L. *Chem. Mater.* **1995**, 7, 333-340.

55. Sheldrick, G.M. TWINABS Acta Cryst. 2008, A64, 112-122.

56. Kepert, D. L. *Prog. Inorg. Chem.* **1978**, *24*, 179-182.

57. Brese, B.N.; O'Keefe, M. **1991**, B47, 192-197.

58. Zhang, X.; Wang, D.; Dou, J.; Yan, S.; Yao, X.; Jiang, J. Inorg. Chem. 2006, 45, 10629-10635.

59. Long, D.; Kogerler, P.; Parenty, A.D.C.; Fielden, J.; Cronin, L. Angew. Chem. Int. Ed. **2006**, 45, 29, 4798-4803.

60. Zhang, S.-Y.; Mao, J.-G. Inorg. Chem. **2011**, 50, 4934-4943.

61. McNeily, C.E. *J. Nucl. Mat.* **1964**, 11, 53-58.

62. Costantini, J.M.; Damien, D.; Novion, C.H.; Blaise, A.; Cousson, A.; Abazli, H.; Pages, M. *J. Solid State Chem.* **1983**, 47, 210-218.

63. Conradson, S.D.; Abney, K.D.; Begg, B.D.; Brady, E.D.; Clark, D.L.; den Auwer, C.; Ding, M.; Dorhout, P.K.; Espinosa-Faller, F.J.; Gordon, P.L.; Haire, R.G.; Hess, N.J.; Hess, R.F.; Keogh, D.W.; Lander, G.H.; Lupinetti, A.J.; Morales, L.A.; Neu, M.P.; Palmer, P.D.; Paviet-Hartmann, P.; Reilly, S.D.; Runde, W.H.; Tait, C.D.; Veirs, D.K.; Wastin, F. *Inorg. Chem.* **2004**, 43, 116-131.

64. Kraft, S.; Stumpel, J.; Becker, P.; Kuetgens, U., *Rev. Sci. Instrum.* **1996**, 67, 681-688.

65. George, G. N.; Kipke, C. A.; Prince, R. C.; Sunde, R. A.; Enemark, J. H.; Cramer, S. P.; *Biochem.* **1989**, 28, 5075-5080.

66. Jalilehvand, F.; Lim, B. S.; Holm, R. H.; Hedman, B.; Hodgson, K. O. *Inorg. Chem.*, **2003**, 42, 5531-5536.

67. Jalilehvand, F.; Mah, V. ; Leung, B. O.; Ross, D.; Parvez, M.; Aroca, R. F. *Inorg. Chem.* **2007**, 46, 4430-4445.

68. Kongmark, C.; Martis, V.; Pirovano, C.; Löfberg, A.; van Beek, W.; Sankar, G.; Rubbens, A. ; Cristol, S.; Vannier, R.-N.; Bordes-Richard, E. *Catalysis Today* **2010**, 157, 257-262.

69. Massa, M.; Häggbladd, R.; Hansen, S.; Andersson, A. *Appl. Catalysis A: General* **2011**, 408, 63-72.

70. Aritani, H.; Tanaka, T.; Funabiki, T.; Yoshida, S.; Kudo, M.; Hasegawa, S. *J. Phys. Chem.* **1996**, 100, 5440-5446.

71. Kutzler, F. W.; Scott, R. A.; Berg, J. M.; Hodgson, K. O.; Doniach, S.; Cramer, S. P.; Chang, C. H. *J. Am. Chem. Soc.* **1981**, 103, 6083-6088.

72. Antonio, M. R.; Teller, R. G.; Sandstrom, D. R.; Mehicic, M.; Brazdil, J. F. *J. Phys. Chem.* **1988**, 92, 2939-2944.

Table 1. Crystallographic Data for $CsPu_3Mo_6O_{24}(H_2O)$ and $Ce_3Mo_6O_{24}(H_2O)_4$.

Compound	**$CsPu_3Mo_6O_{24}(H_2O)$**	**$Ce_3Mo_6O_{24}(H_2O)_4$**
Formula Mass	1850.55	1455.0
Color and habit	Black, plate	Yellow, plate
Space group	*C*2/*c*	*C*2/*c*
a (Å)	12.633(5)	12.7337(7)
b (Å)	21.770(8)	22.1309(16)
c (Å)	7.743(7)	7.8392(4)
a (°)	90	90
β (°)	96.218(2)	96.591(4)
γ(°)	90	90
V (ÅP^{3P})	2117(2)	2194.6(2)
Z	4	4
T (K)	100	100
λ (Å)	0.71073	0.71073
Maximum 2q (deg.)	27.48	27.53
ρB_{calcdB} (g cm^{-3})	5.806	4.380
μ(Mo *K*a) (cm^{-1})	1444.1	951.7
$R(F)$ for $F_o^2 > 2s(F_o^2)^a$	0.0417	0.0403
$R_w(F_o^2)^b$	0.0626	0.0632

[a] $R(F) = \Sigma \left\| F_o \right| - \left| F_c \right\| / \Sigma \left| F_o \right|$. [b] $R_w(F_o^2) = \left[\Sigma \left[w\left(F_o^2 - F_c^2\right)^2 \right] / \Sigma\, w F_o^4 \right]^{1/2}$.

Table 2. Selected Bond Distances for PuMoO and CeMoO.

$Ce_3Mo_6O_{24}(H_2O)_4$		$CsPu_3Mo_6O_{24}(H_2O)$	
Ce(1)-O(10)	2.229(6)	Pu(1)-O(3)	2.257(11)
Ce(1)-O(10)	2.229(6)	Pu(1)-O(3)	2.257(11)
Ce(1)-O(1)	2.283(6)	Pu(1)-O(2)	2.315(9)
Ce(1)-O(1)	2.283(6)	Pu(1)-O(2)	2.315(9)
Ce(1)-O(7)	2.325(6)	Pu(1)-O(11)	2.320(9)
Ce(1)-O(7)	2.325(6)	Pu(1)-O(11)	2.320(9)
Ce(1)-O(1)	2.514(6)	Pu(1)-O(11)	2.410(8)
Ce(1)-O(1)	2.514(6)	Pu(1)-O(11)	2.410(8)
Ce(2)-O(5)	2.231(6)	Pu(2)-O(4)	2.234(11)
Ce(2)-O(11)	2.242(7)	Pu(2)-O(9)	2.257(10)
Ce(2)-O(2)	2.283(6)	Pu(2)-O(1)	2.313(8)
Ce(2)-O(6)	2.295(6)	Pu(2)-O(7)	2.322(9)
Ce(2)-O(3)	2.339(6)	Pu(2)-O(10)	2.369(9)
Ce(2)-O(4)	2.406(6)	Pu(2)-O(6)	2.372(8)
Ce(2)-O(4)	2.425(6)	Pu(2)-O(1)	2.427(8)
Ce(2)-O(6)	2.482(6)	Pu(2)-O(6)	2.433(8)
Mo(1)-O(9)	1.689(7)	Mo(1)-O(5)	1.660(12)
Mo(1)-O(7)	1.774(6)	Mo(1)-O(2)	1.758(9)
Mo(1)-O(6)	1.860(6)	Mo(1)-O(1)	1.860(8)
Mo(1)-O(10)	1.955(6)	Mo(1)-O(3)	1.940(10)
Mo(1)-O(5)	2.096(6)	Mo(1)-O(4)	2.090(10)
Mo(2A)-O(8)	1.608(7)	Mo(2A)-O(8)	1.667(14)
Mo(2A)-O(2)	1.791(6)	Mo(2A)-O(7)	1.741(8)
Mo(2A)-O(4)	1.877(6)	Mo(2A)-O(6)	1.882(9)
Mo(2A)-O(11)	2.027(7)	Mo(2A)-O(9)	2.013(11)
Mo(2A)-O(11)	2.061(6)	Mo(2A)-O(9)	2.089(10)
Mo(2B)-O(2)	1.717(6)	Mo(3A)-O(12)	1.686(13)
Mo(2B)-O(13B)	1.74(2)	Mo(3A)-O(10)	1.738(9)
Mo(2B)-O(4)	1.846(6)	Mo(3A)-O(11)	1.884(9)
Mo(2B)-O(11)	1.973(7)	Mo(3A)-O(4)	1.928(11)
Mo(2B)-O(11)	2.143(7)	Mo(3A)-O(3)	2.112(9)
Mo(2B)-O(13A)	2.360(14)	Mo(2B)-O(6)	1.856(9)
Mo(3A)-O(13A)	1.711(12)	Mo(2B)-O(7)	1.873(10)
Mo(3A)-O(3)	1.783(6)	Mo(2B)-O(9)	2.056(11)
Mo(3A)-O(1)	1.831(6)	Mo(2B)-O(9)	2.234(12)
Mo(3A)-O(5)	1.938(6)	Mo(3B)-O(10)	1.738(12)
Mo(3A)-O(10)	2.134(6)	Mo(3B)-O(11)	1.757(11)
Mo(3A)-O(13B)	2.22(2)	Mo(3B)-O(13B)	1.83(2)
Mo(3A)-O(12)	2.504(7)	Mo(3B)-O(4)	2.091(14)
Mo(3B)-O(12)	1.503(8)	Mo(3B)-O(13A)	2.203(16)
Mo(3B)-O(3)	1.791(6)	Mo(3B)-O(3)	2.334(12)
Mo(3B)-O(1)	1.901(6)	Mo(3B)-O(13A)	2.361(15)

a.

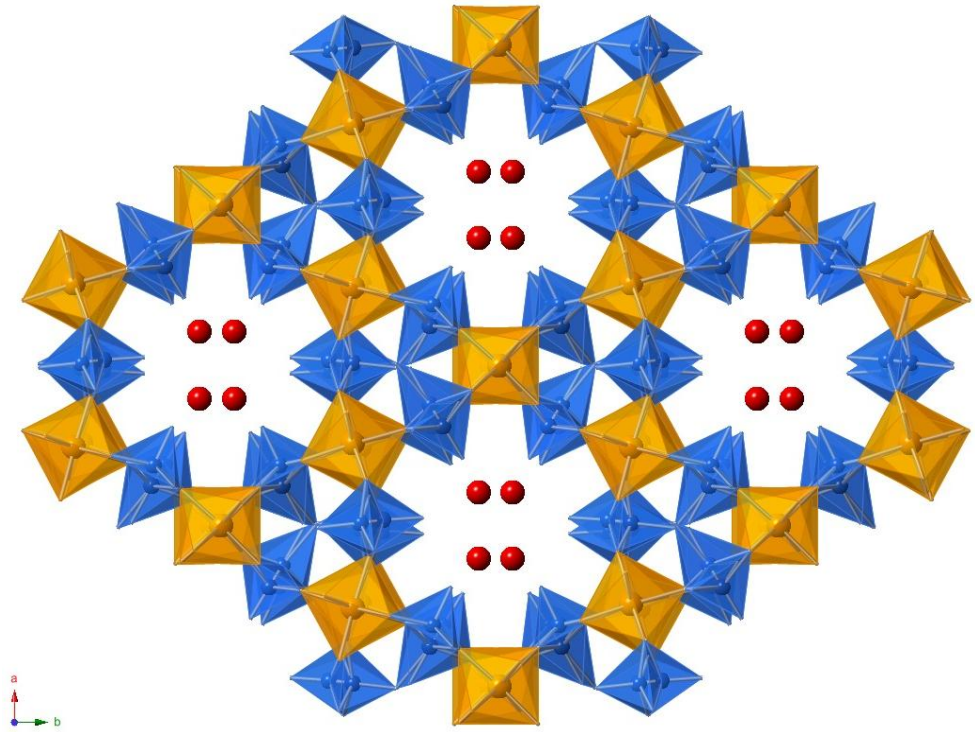

b.

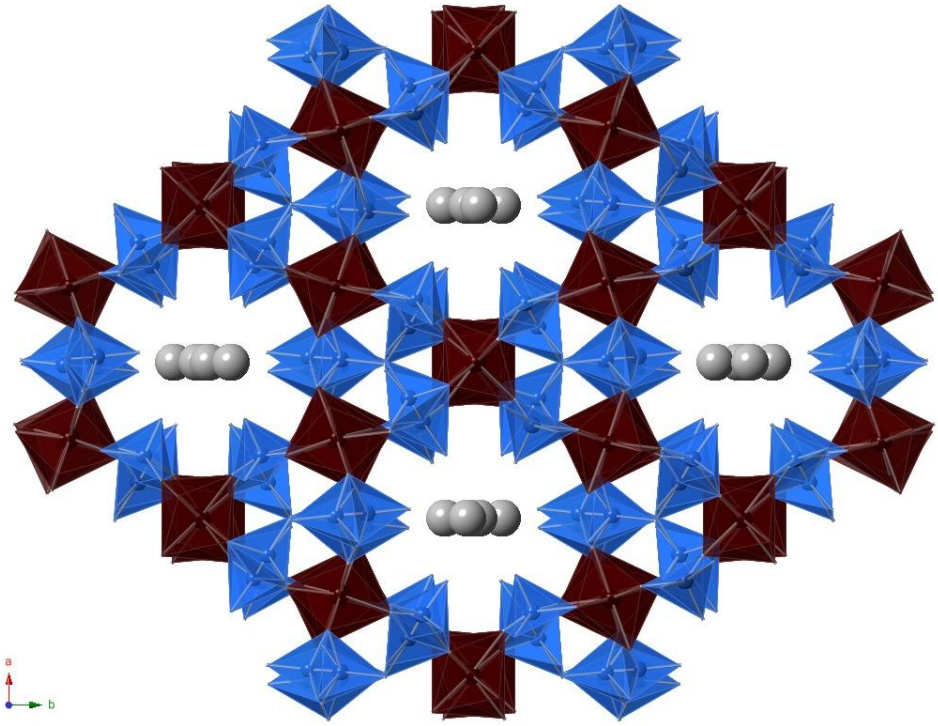

Figure 1 View down the *c* axis of $Ce_3Mo_6O_{24}(H_2O)_4$ (**a.**) and $CsPu_3Mo_6O_{24}(H_2O)$ (**b.**). Ce(IV) polyhedra are orange, Pu(IV) polyhedra are dark red, molybdate polyhedra are blue, oxygen atoms are red spheres, and Cs atoms are grey spheres.

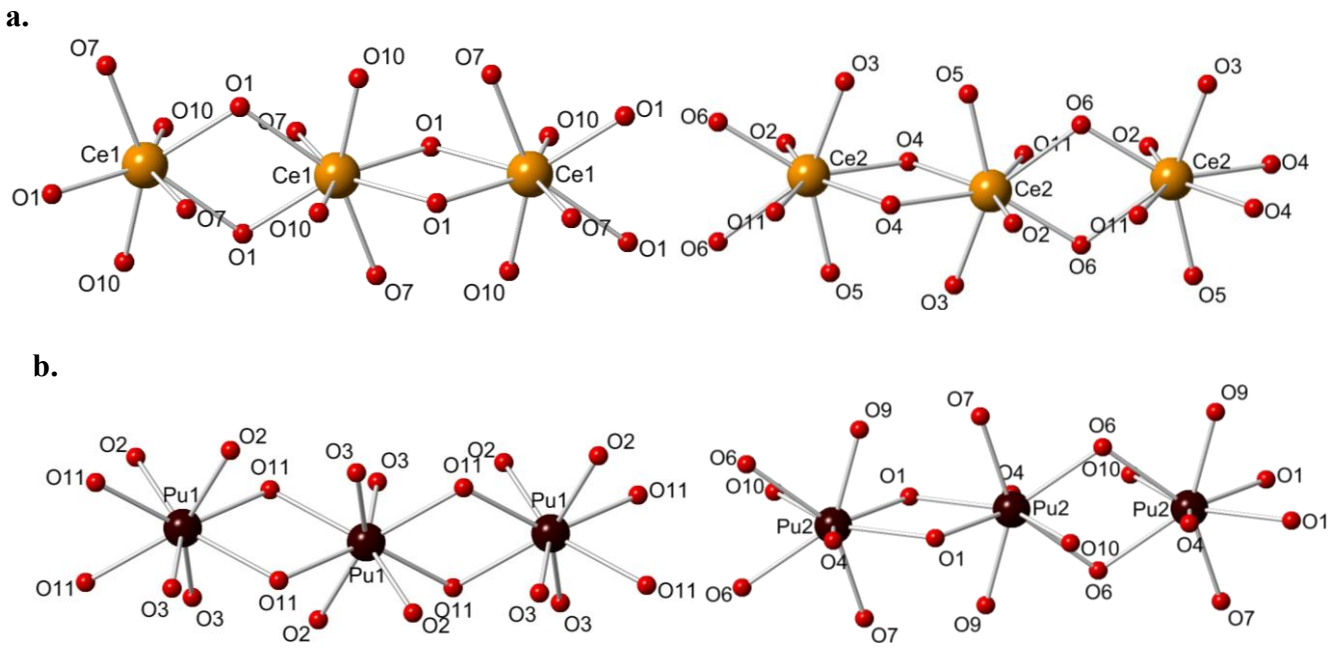

Figure 2. The coordination environments of the Ce(IV) (orange spheres) and Pu(IV) (dark red spheres) metal centers consisting of alternating edge sharing chains. All coordination environments are eight-coordinate square anti-prisms with approximate D_{4d} symmetry. The chains are linked by molybdate polyhedra to build the framework.

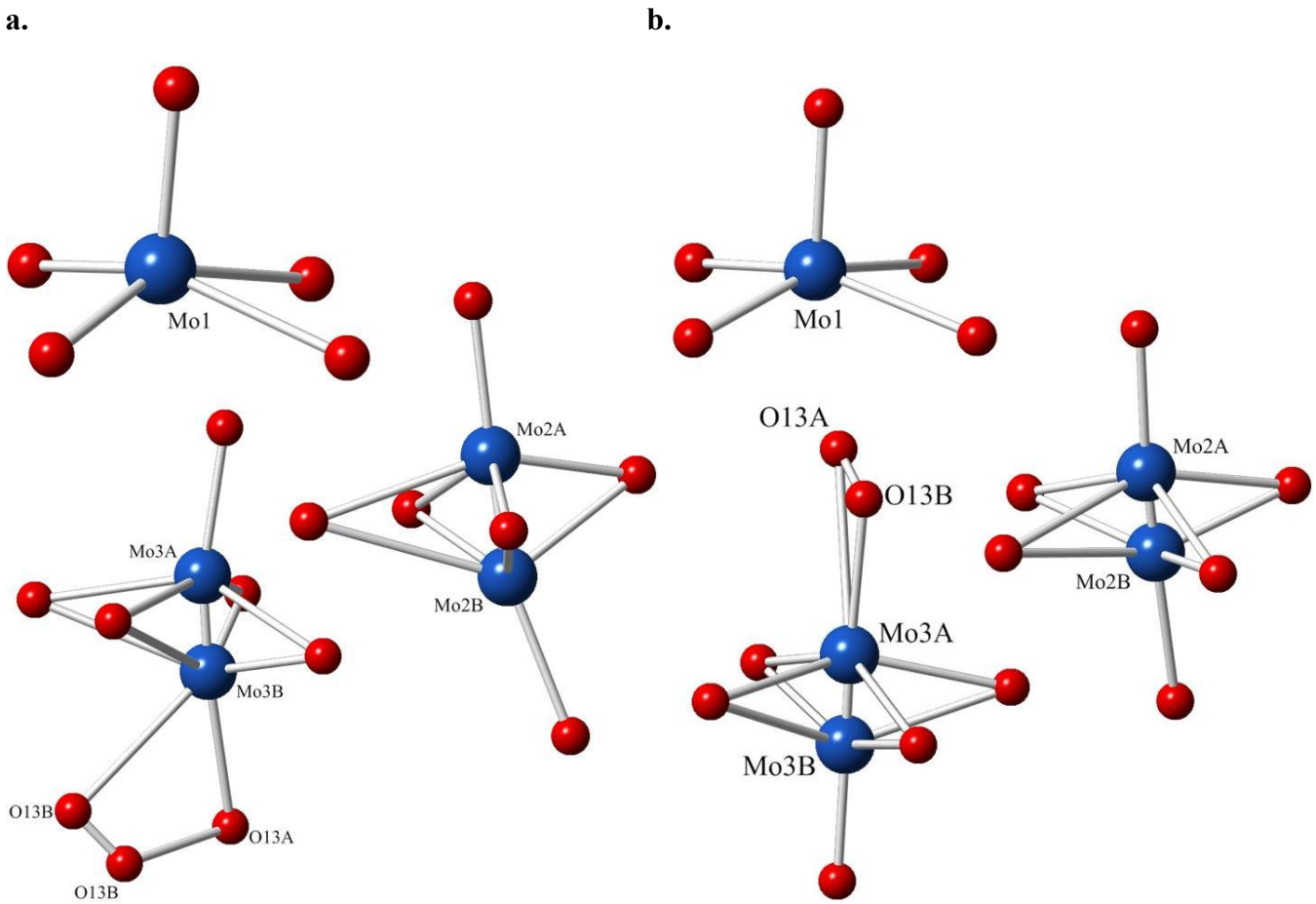

Figure 3. Coordination environments of Mo in $CsPu_3Mo_6O_{24}(H_2O)$ (**a.**) and the coordination environment of Mo in $Ce_3Mo_6O_{24}(H_2O)_4$ (**b.**). The square pyramid of Mo1 is not disordered in either structure but the other molybdate units are disordered over two sites with 25% occupancy for Mo(2B) and 25% occupancy for Mo(3B). The disordered O(13) is also shown. Blue spheres represent Mo atoms and red spheres represent O atoms.

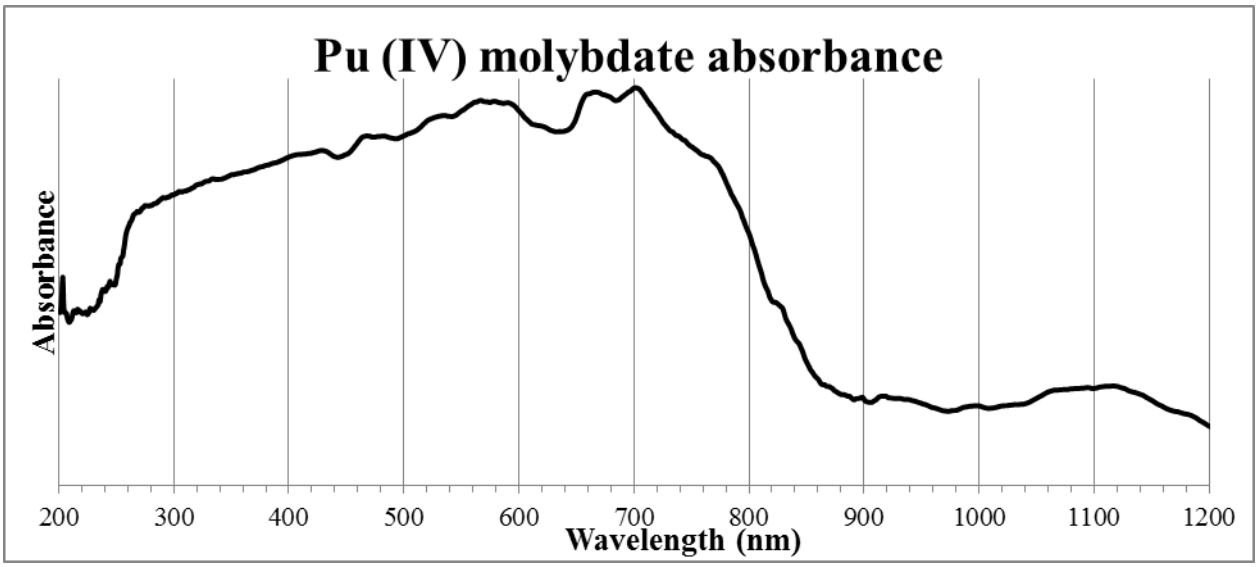

Figure 4. Absorption spectrum of $CsPu_3Mo_6O_{24}(H_2O)$ showing the strong absorbance from approximately 250 nm to 800 nm. The typical f-f transition analysis fails here since those features are overwhelmed.

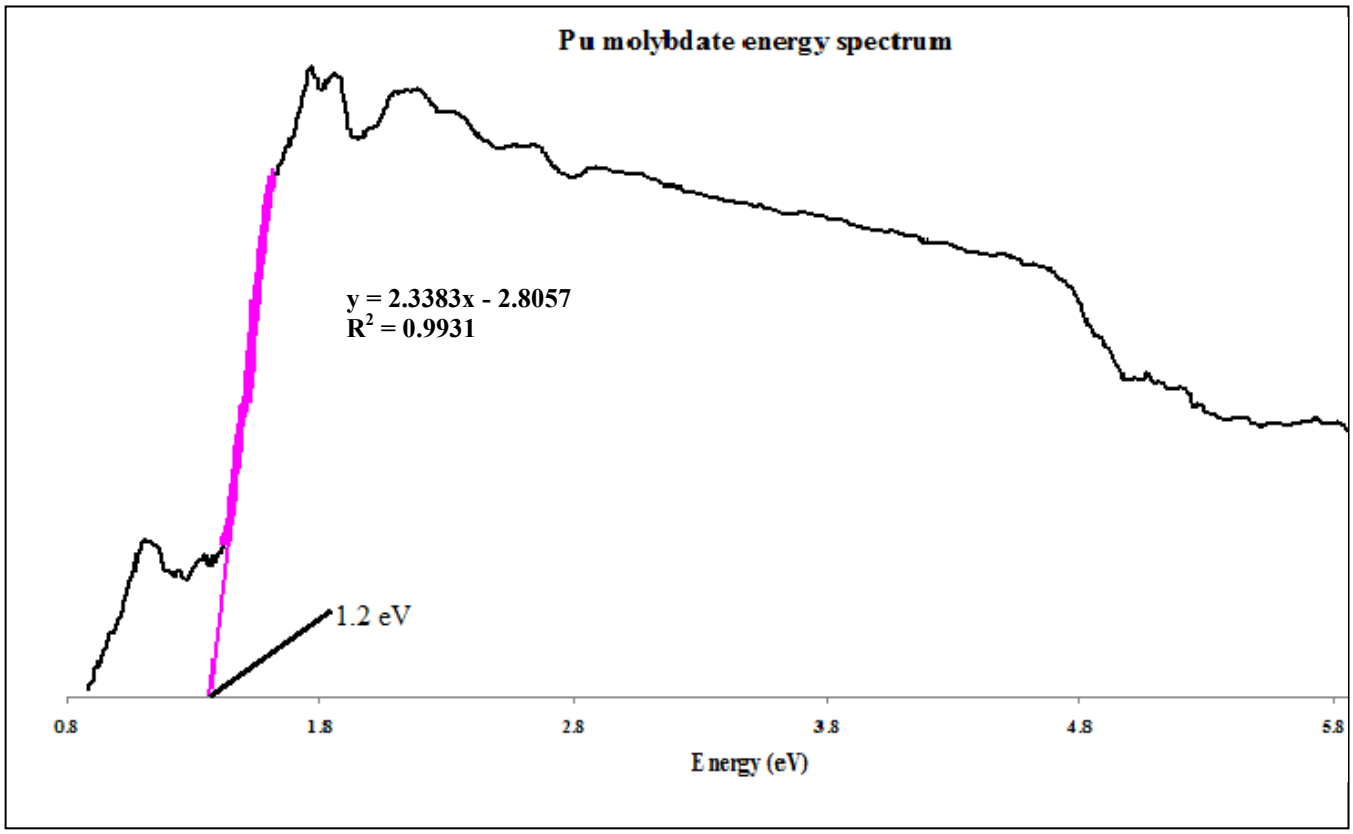

Figure 5. Optical energy spectra of $CsPu_3Mo_6O_{24}(H_2O)$ used to determine the approximate bandgap. The least squares fit of the highlighted region is shown along with the x-intercept that is the calculated bandgap.

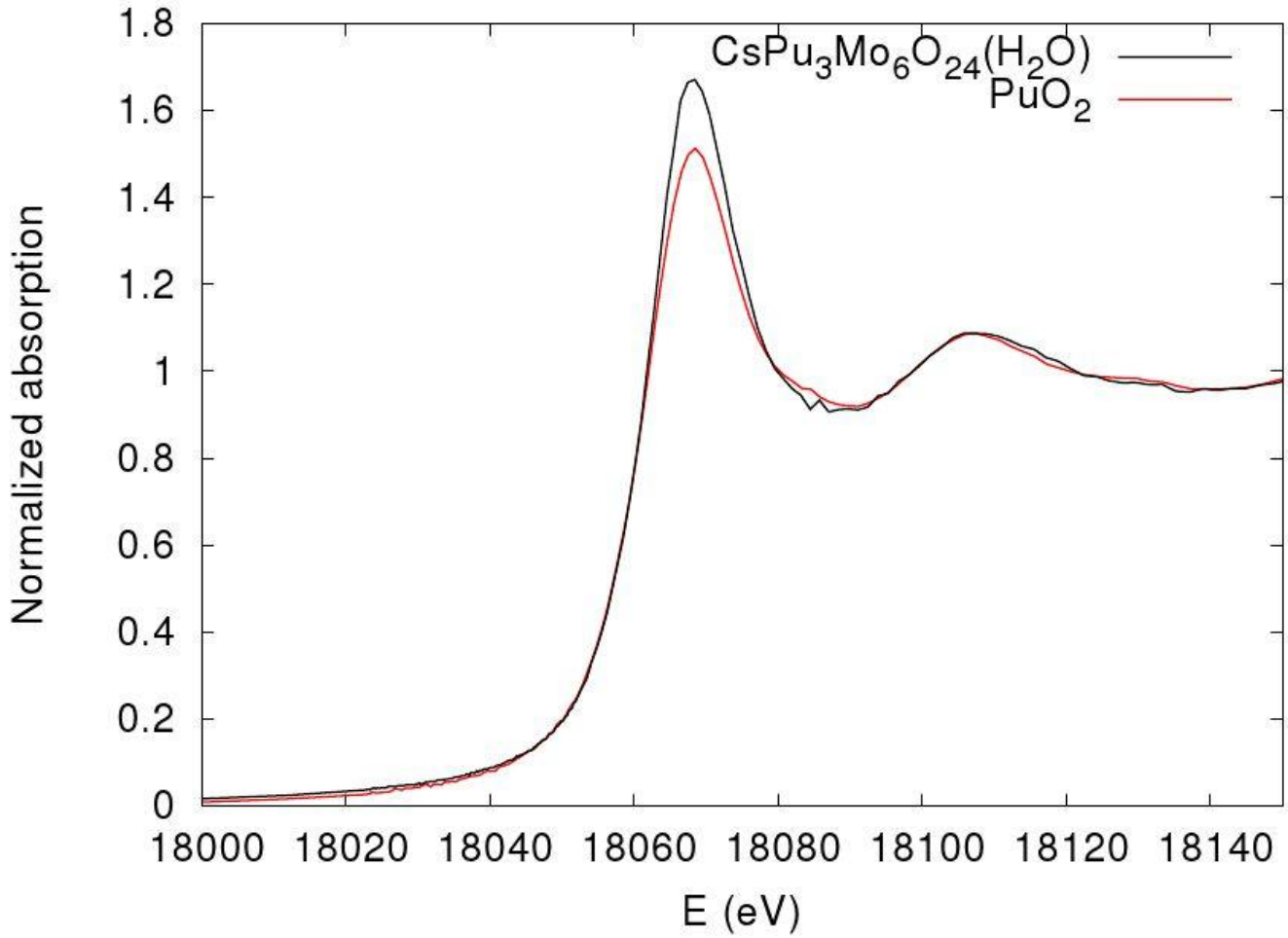

.

Figure 6. Pu XANES comparing the standard $Pu(IV)O_2$ to $CsPu_3Mo_6O_{24}(H_2O)$ indicating that Pu is in the tetravalent state.

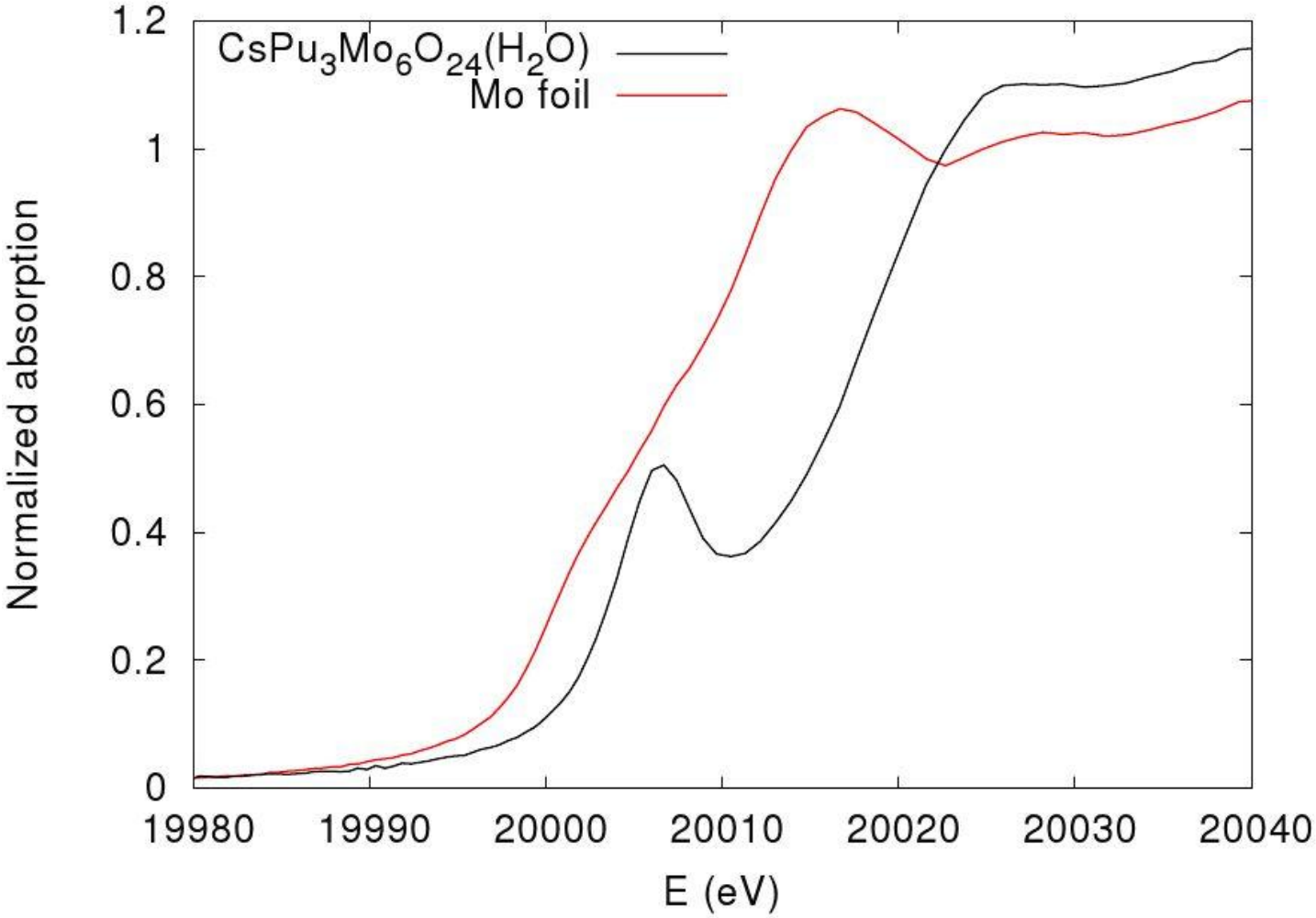

Figure 7. Mo K-edge XANES exhibits a substantial pre-edge absorption peak making analysis difficult however, the energy at half-height of the edge indicates a Mo(V) or Mo(VI) valence.

TOC

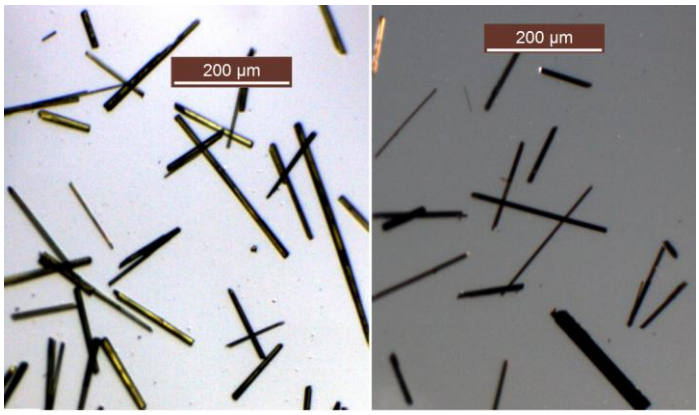

DISCLAIMER

This document was prepared as an account of work sponsored by the United States Government. While this document is believed to contain correct information, neither the United States Government nor any agency thereof, nor the Regents of the University of California, nor any of their employees, makes any warranty, express or implied, or assumes any legal responsibility for the accuracy, completeness, or usefulness of any information, apparatus, product, or process disclosed, or represents that its use would not infringe privately owned rights. Reference herein to any specific commercial product, process, or service by its trade name, trademark, manufacturer, or otherwise, does not necessarily constitute or imply its endorsement, recommendation, or favoring by the United States Government or any agency thereof, or the Regents of the University of California. The views and opinions of authors expressed herein do not necessarily state or reflect those of the United States Government or any agency thereof or the Regents of the University of California.